Research article

LUMINESCENCE
The Journal of Biological and Chemical Luminescence

Received: 09 November 2013, Accepted: 19 February 2014 Published online in Wiley Online Library

(wileyonlinelibrary.com) DOI 10.1002/bio.2668

Synthesis and fluorescence properties of 1,2,4-triazolo[3,4-b]-1,3,4-thiadiazol derivatives and their terbium complexes

Wu Zhang,[a] Yuchao Chai,[a] Kangyun Li,[a] Yanwen Chen,[b] Dong Yan[a] and Dongcai Guo[a]*

ABSTRACT: Eight novel 1,2,4-triazolo[3,4-b]-1,3,4-thiadiazol derivatives have been designed and synthesized, and their corresponding Tb^{3+} complexes were also prepared successfully. The fluorescence properties and fluorescence quantum yields of the target complexes were investigated, the results showed that the ligands were an efficient sensitizer for Tb^{3+} luminescence, and the target complexes exhibited characteristic fluorescence emissions of Tb^{3+} ion. The fluorescence intensity of the complex substituted by chlorine was stronger than that of other complexes. The substituents' nature has a great effect upon the electrochemical properties of the target complexes. The results showed that the introduction of the electron-withdrawing groups tended to decrease the oxidation potential and highest occupied molecular orbital energy levels of the target Tb^{3+} complexes; however, introduction of the electron-donating groups can increase the corresponding complexes' oxidation potential and highest occupied molecular orbital energy levels. Copyright © 2014 John Wiley & Sons, Ltd.

Keywords: 1,2,4-Triazoles; synthesis; terbium complex; fluorescence properties; electrochemical properties

Introduction

Rare earth complexes are the subject of increasing interest in bioinorganic and coordination chemistry because of their successful application as diagnostic tools in biomedical analysis, laser systems, optical amplification, etc. (1–4). Luminescence of rare earth complexes results from the unique 4f orbitals, which are well shielded by the outer $5s^2$ and $5p^6$ electrons (5–7). Therefore, the luminescence excited directly from the rare earth ions is unfavorable and so, it is very important to design and synthesize novel ligands possessing high absorption efficiency.

Sujith *et al.* (8) has synthesized a series of 1,2,4-triazolo[3,4-b]-1,3,4-thiadiazol derivatives, which represent one of the most biologically active classes of compounds, possessing a wide spectrum of pharmacological activities, but, few studies exist of 1,2,4-triazolo[3 ,4-b]-1,3,4-thiadiazol derivatives as ligands, synthesis and applications in rare earth complexes. This motivated our research interest in Tb^{3+} complexes based on 1,2,4-triazolo[3,4-b]-1,3,4-thiadiazol. Because the 1,2,4-triazolo[3,4-b]-1,3,4-thiadiazol derivatives present appropriate π-conjugated system, good planarity and a variety of coordination sites, it is possible in theory that they would be good organic ligands. However, studies are needed to prove whether these kinds of ligands possess highly efficient energy transfer (9).

In this work, compounds containing the 1,2,4-triazolo [3,4-b]-1,3,4-thiadiazol were designed and synthesized, and their corresponding Tb^{3+} complexes were also prepared. The fluorescence properties of target complexes were studied in detail and the fluorescence quantum yields of the Tb^{3+} complexes was also investigated. Meanwhile, the relationship between the structure of ligands and the electrochemical properties of the target complexes were discussed in detail. The synthesis route for the 1,2,4-triazolo[3,4-b]-1,3,4-thiadiazol derivatives (L^{1-8}) is shown in Scheme 1.

Experimental

Materials and methods

Pyridine-2,6-dicarboxylic acid (purity 99.99%, Entai Science and Technology Co., Ltd. Wuhan, China) and Tb_2O_3 (purity 99.99%) were purchased from commercial suppliers. $Tb(NO_3)_3$ (0.2 mol/L) solution was prepared by dissolving Tb_2O_3(99.99%) in HNO_3 according to the literature (10). Monochloroacetic acid (Sinopharm Group Co., Ltd. China) and ethyl acetate were of C.P. grade, phenol derivatives and other chemicals were of A.R. grade and used without purification.

Proton nuclear magnetic resonance (^{1}H NMR) spectra was recorded in dimethyl sulfoxide (DMSO)-d_6/$CDCl_3$ on Brucker spectrophotometer (America) (400 MHz) with TMS as an internal standard. Infrared (IR) spectra (400–4000/cm) were obtained in KBr discs by a Perkin-Elmer Spectrum One (PERKIN-ELMER). Ultraviolet (UV) spectra (190–450 nm) were recorded by LabTech UV-2100 (LabTech) spectrophotometer, with DMSO as solvent and reference. Elemental analysis of the complexes was carried out on a VarioEL 111 CHNS (Germany) analyzer. Melting points

* Correspondence to: Dongcai Guo, Dongcai Guo School of Chemistry and Chemical Engineering, Hunan University, Changsha 410082, China. E-mail: dcguo2001@hnu.edu.cn

[a] School of Chemistry and Chemical Engineering, Hunan University, Changsha 410082, China

[b] Institute of Nonferrous Metallurgy Labor Protection, Hunan, Changsha 410014, China

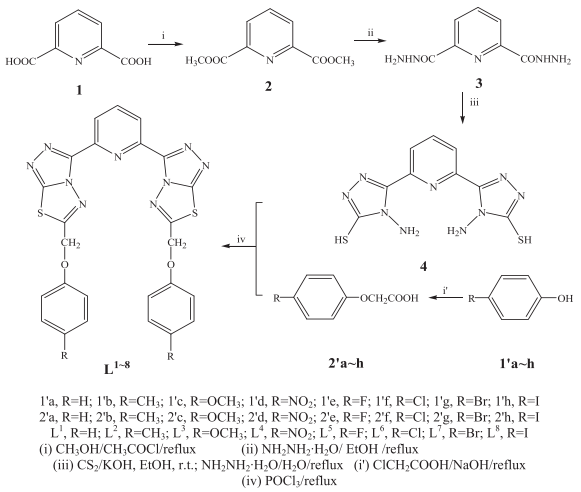

1'a, R=H; 1'b, R=CH_3; 1'c, R=OCH_3; 1'd, R=NO_2; 1'e, R=F; 1'f, R=Cl; 1'g, R=Br; 1'h, R=I
2'a, R=H; 2'b, R=CH_3; 2'c, R=OCH_3; 2'd, R=NO_2; 2'e, R=F; 2'f, R=Cl; 2'g, R=Br; 2'h, R=I
L^1, R=H; L^2, R=CH_3; L^3, R=OCH_3; L^4, R=NO_2; L^5, R=F; L^6, R=Cl; L^7, R=Br; L^8, R=I
(i) CH_3OH/CH_3COCl/reflux (ii) $NH_2NH_2{\cdot}H_2O$/ EtOH /reflux
(iii) CS_2/KOH, EtOH, r.t.; $NH_2NH_2{\cdot}H_2O/H_2O$/reflux (i') $ClCH_2COOH$/NaOH/reflux
(iv) $POCl_3$/reflux

Scheme 1. The synthetic route for the ligand $\mathbf{L^{1\sim8}}$.

of all compounds were determined on an X-4 binocular microscope. The thermal gravimetric analysis was carried out on a NETZSCH STA 409PC thermal gravimetric analyzer (Germany). In the cyclic voltammetry curve testing three electrodes were used (glassy electrode, platinum electrode and a saturated calomel electrode), ferrocene was used as an external standard, nitrite solution as the supporting electrolyte and DMSO as the solvent; the test scanning speed was 100 mV/s and the sensitivity was 1 mA. The fluorescence spectra were measured by using powder samples on a Hitachi F-2700 Fluorescence Spectrophotometer (Japan) at room temperature. The width of excitation and emission slits were both 2.5 nm.

General procedure for synthesis of the intermediates

Synthesis of compound 2. A solution of 2,6-pyridine dicarboxylic acid (60 mmol, 10.02 g) in anhydrous methanol (80 mL) was added to a 150 mL three-neck flask and then the acetyl chloride was gradually added dropwise while stirring in the ice water bath (11). The reaction mixture was heated and refluxed for 24 h with stirring in the oil bath. The formed precipitate was collected by filtration, washed several times with ethyl acetate and dried at room temperature. The white powder of compound **2** was obtained. Yield was 91%.

Synthesis of compound 3. A mixture of compound **2** (53 mmol) in absolute ethanol (200 mL) was added to a 500 mL three-neck flask and refluxed for some time, until the temperature was maintained to 85 °C. The hydrazine hydrate (30 mL, 85%) was added to the refluxing mixture. The resulting mixture was further allowed to reflux for 6 h. Excess ethanol was distilled out under reduced pressure and diluted with water. The precipitate were formed and stood for some time, and then the reaction mixture was filtered, thoroughly washed with cold water and recrystallized from water. Yield was 92%.

Synthesis of compound 4. Potassium hydroxide (20 mmol) was dissolved in absolute ethanol (30 mL). The resulting solution was cooled in ice bath, and compound **3** (5 mmol, 0.98 g) was added with stirring. A solution of carbon disulfide (20 mmol, 1.52 g) in anhydrous ethanol was added while stirring. Most of the precipitate appeared after dropped and then diluted with 10 mL of anhydrous ethanol. The reaction mixture was agitated continuously for 14 h at room temperature, and then the ether (30 mL) was added and stirring was continued for 30 min. The precipitated potassium dithiocarbazinate was collected by filtration, washed with anhydrous ether two times and dried in a vacuum for 24 h. Thus, the potassium salt was obtained and used in the next step without further purification (12).

A suspension of potassium dithiocarbazinate in water (2 mL) and hydrazine hydrate (85%, 2 mL) were added into a 100 mL single-necked flask and heated for 6 h at 110 °C. The resulting mixture was cooled to room temperature and gradually poured on to crushed ice (30 mL) with stirring. The color of the reaction mixture changed to reddish brown. The pH value of the solution was adjusted to 6.0 by dropwise addition of aqueous HCl. The white precipitate was obtained during the reaction process and allowed to stand overnight. The resulting solid was dissolved in a solution of a mixture (30 mL) of water and ethanol (1 : 1). The reaction mixture was heated to boiling while stirring; a white solid was obtained by hot filtration and dried in vacuum for 24 h. Yield was 20%.

Synthesis of phenoxyacetic acid derivatives 2′a–h. The procedures for synthesis of compounds **2′a–h** were carried out according to the literature (10) and partly revised by ourselves. As the synthesis methods of compounds **2′a–h** were similar, only the synthesis process of the phenoxyacetic acid compound **2′a** was described as an example. The solution of sodium monochloroacetate was obtanied that a solution of monochloroacetic acid (0.05 mmol, 4.72 g) in water (20 mL) was cooled in an ice bath and then the sodium hydroxide (25%) added with stirring. Thus, a solution of sodium monochloroacetate was obtained when the pH value was 9–10. The mixture of sodium hydroxide (0.04 mol, 1.60 g), water (20 mL), ethanol (5 mL) and phenol (0.04 mol, 3.76 g) were added portionwise into a 150 mL three-neck flask and then the above solution of sodium monochloroacetate was slowly added. The reaction mixture was refluxed at 105 °C for 5 h. The resulting solution was cooled to room temperature and acidified with dilute hydrochloric acid until the pH value reached 1–2. At that moment, a large number of white precipitate was formed, and then filtered off, washed several times with HCl and dried in vacuum. Thus, the white solid of phenoxyacetic acid was obtained.

Phenoxyacetic acid (2′a). White crystals, yield 67%. ^{1}H NMR (400 MHz, $CDCl_3$), δ/ppm: 4.70 (s, 2H, CH_2), 6.94 (d, 2H, J = 8.0 Hz, ArH), 7.02–7.05 (t, 1H, J = 7.2 Hz, ArH), 7.30–7.35 (m, 2H, ArH); MS(ESI) m/z (%): 304 (2 M, 13), 303 (2 M – 1, 100), 151 (M – 1, 28).

p-*Tolyloxyacetic acid (2′b)*. White crystals, yield 69%. ^{1}H NMR (400 MHz, $CDCl_3$), δ/ppm: 2.30 (s, 3H, CH_3), 4.66 (s, 2H, CH_2), 6.83 (d, 2H, J = 8.8 Hz, ArH), 7.12 (d, 2H, J = 8.8 Hz, ArH); MS (EI) m/z (%): 167 (M + 1, 10), 166 (M, 100), 121 (60), 107 (50), 91 (64), 77 (26), 65 (17).

(4-Methoxy-phenoxy)-acetic acid (2′c). White crystals, yield 68%. ^{1}H NMR (400 MHz, $CDCl_3$), δ/ppm:3.78 (s, 3H, CH_3), 4.63 (s, 2H, CH_2), 6.84–6.86 (m, 2H, ArH), 6.87–6.90 (m, 2H, ArH); MS (EI) m/z (%): 183 (M + 1, 6), 182 (M, 64), 123 (100), 109 (16), 95 (26), 92 (9), 77 (8).

(4-Nitro-phenoxy)-acetic acid (2′d). White powder, yield 72%. ^{1}H NMR (400 MHz, DMSO-d_6), δ/ppm: 4.88 (s, 2H, CH_2), 7.13–7.15 (t, 2H, ArH), 8.20–8.22 (t, 2H, ArH); MS (EI) m/z (%): 198 (M + 1, 9), 197 (M, 100), 181 (3), 167 (17), 152 (85), 139 (11), 122 (22), 109 (38), 92 (29), 76 (18).

(4-Fluoro-phenoxy)-acetic acid (2′e). White crystals, yield 52%. ^{1}H NMR (400 MHz, $CDCl_3$), δ/ppm: 4.67 (s, 2H, CH_2), 6.87–6.90 (m, 2H,

LUMINESCENCE
The Journal of Biological and Chemical Luminescence

ArH), 6.99–7.03 (m, 2H, ArH); MS (EI) m/z (%): 171 (M + 1, 9), 170 (M, 100), 125 (79), 112 (41), 95 (68), 83 (30), 75 (17).

(4-Chloro-phenoxy)-acetic acid (2′f). White crystals, yield 85%. ^{1}H NMR (400 MHz, $CDCl_3$), δ/ppm: 4.67 (s, 2H, CH_2), 6.87 (d, 2H, J = 8.8 Hz, ArH), 7.27 (d, 2H, J = 8.4 Hz, ArH); MS (EI) m/z (%): 188 (M + 2, 32), 186 (M, 100), 141 (79), 128 (56), 111 (59), 99 (32), 75 (33).

(4-Bromo-phenoxy)-acetic acid (2′g). White powder, yield (78%). ^{1}H NMR (400 MHz, $CDCl_3$), δ/ppm: 4.76 (s, 2H, CH_2), 6.82 (d, 2H, J = 9.2 Hz, ArH), 7.42 (d, 2H, J = 9.2 Hz, ArH); MS (EI) m/z (%): 232 (M + 1, 97), 230 (M – 1, 100), 187 (47), 185 (49), 174 (34), 172 (37), 157 (40), 155 (35), 143 (17), 76 (20).

(4-Iodo-phenoxy)-acetic acid (2′h). White powder, yield 76%. ^{1}H NMR (400 MHz, $CDCl_3$), δ/ppm: 4.67 (s, 2H, CH_2), 6.71 (d, 2H, J = 9.2 Hz, ArH), 7.60 (d, 2H, J = 8.4 Hz, ArH); MS (EI) m/z (%): 279 (M + 1, 9), 278 (M, 100), 233 (23), 220 (21), 203 (15), 191 (7), 106 (6), 92 (6), 76 (11).

Synthesis of 1,2,4-triazolo[3,4-b]-1,3,4-thiadiazol derivatives L^{1-8}. As the synthesis methods of the compounds L^{1-8} were similar, the synthesis of compound L^1 was described as an example. In the 100 mL single-necked flask, both compound **4** (2 mmol, 0.61 g) and phenoxyacetic acid (6 mmol, 0.91 g) were dissolved in 15 mL of dry phosphorous oxychloride. The resulting solution was refluxed at 106 °C for 7 h. Excess of $POCl_3$ was removed by vacuum distillation. The reaction mixture was cooled to room temperature and then gradually poured into 400 mL of crushed ice while stirring. The potassium hydroxide solution (2 mol/L) was added until the pH value of the mixture raised to 8. The resulting mixture was allowed to stand overnight and precipitate completely, then filtered, washed thoroughly with cold water, dried and recrystallized from anhydrous ethanol to give the target compound L^1.

2,6-bis(6-(phenoxymethyl)-[1,2,4]triazolo[3,4-b][1,3,4]thiadiazol-3-yl)pyridine (L^1). Brown solid, yield 81%. m.p. 192 °C; ^{1}H NMR (400 MHz, $CDCl_3$), δ/ppm: 5.45 (s, 4H, CH_2), 6.98–7.00 (dd, 4H, J_1 = 8.8 Hz, J_2 = 0.8 Hz, ArH), 7.06–7.10 (m, 2H, ArH), 7.31–7.35 (m, 4H, ArH), 8.11–8.15 (t, 1H, J = 7.8Hz, pyridine proton), 8.49 (d, 2H, J = 8 Hz, pyridine protons); IR (KBr) v/cm: 3138, 1598, 1573, 1540, 1454, 1401, 1246, 1080, 690; MS (ESI) m/z (%): 1079 (2 M-1, 47), 563 (M + 23, 15), 562 (M + 22, 53), 540 (M, 51); Anal. Calcd. for $C_{25}H_{17}N_9O_2S_2$: C, 55.65; H, 3.18; N, 23.36; S, 11.88. Found: C, 55.25; H, 3.62; N, 23.75; S, 11.46.

2,6-bis(6-(p-tolyloxymethyl)-[1,2,4]triazolo[3,4-b][1,3,4]thiadiazol-3-yl)pyridine (L^2). Brown solid, yield 92%. m.p. 205 °C; ^{1}H NMR (400 MHz, $CDCl_3$), δ/ppm: 2.31 (s, 6H, CH_3), 5.41 (s, 4H, CH_2), 6.88 (d, 4H, J = 8.8 Hz, ArH), 7.06–7.15 (m, 4H, ArH), 8.10–8.14 (t, 1H, J = 7.8Hz, pyridine proton), 8.48 (d, 2H, J = 8.0 Hz, pyridine protons); IR (KBr) v/cm: 3122, 2860, 1590, 1574, 1542, 1458, 1401, 1241, 1083, 685; MS (ESI) m/z (%): 1157 (2 M + 21, 100), 1135 (2 M – 1, 40), 590 (M + 22, 58), 568 (M, 47); Anal. Calcd. for $C_{27}H_{21}N_9O_2S_2$: C, 57.13; H, 3.73; N, 22.21; S, 11.30. Found: C, 57.35; H, 3.57; N, 22.15; S, 11.12.

2,6-bis(6-((4-methoxyphenoxy)methyl)-[1,2,4]triazolo[3,4-b][1,3,4]thiadiazol-3-yl)pyridine (L^3). Brown solid, yield 63%. m.p. 191 °C; ^{1}H NMR (400 MHz, $CDCl_3$), δ/ppm: 3.77 (s, 6H, OCH_3), 5.38 (s, 4H, CH_2), 6.84 (d, 4H, 8.8 Hz, ArH), 6.92 (d, 4H, J = 9.2 Hz, ArH), 8.10–8.14 (t, 1H, J = 7.8 Hz, pyridine proton), 8.48 (d, 2H, J = 8.0 Hz, pyridine protons); IR (KBr) v/cm: 3121, 1594, 1574, 1460, 1401, 1232, 1109, 1032, 688; MS (ESI) m/z (%): 623 (M + 23, 38), 622 (M + 22, 100); Anal. Calcd. for $C_{27}H_{21}N_9O_4S_2$: C, 54.08; H, 3.53; N, 21.02; S, 10.69. Found: C, 54.50; H, 3.58; N, 20.53; S, 10.67.

2,6-bis(6-((4-nitrophenoxy)methyl)-[1,2,4]triazolo[3,4-b][1,3,4]thiadiazol-3-yl)pyridine (L^4). White solid, yield 60%. m.p. 310 °C; ^{1}H NMR (400 MHz, $CDCl_3$) δ/ppm: 5.47 (s, 4H, CH_2), 7.21 (t, 4H, ArH), 8.33 (t, 4H, ArH), 8.13–8.18 (t, 1H, J = 6.0 Hz, pyridine proton), 8.48 (d, 2H, J = 6.0 Hz, pyridine protons); IR (KBr) v/cm: 3119, 1611, 1544, 1509, 1466, 1400, 1259, 1054, 687; MS (ESI) m/z (%): 653 (M + 23, 36), 652 (M + 22, 100), 630 (M, 22); Anal. Calcd. for $C_{25}H_{15}N_{11}O_6S_2$: C, 47.69; H, 2.40; N, 24.47; S, 10.19. Found: C, 47.88; H, 2.41; N, 24.68; S, 10.14.

2,6-bis(6-((4-fluorophenoxy)methyl)-[1,2,4]triazolo[3,4-b][1,3,4]thiadiazol-3-yl)pyridine (L^5). Gray solid, yield 92%. m.p. 228 °C; ^{1}H NMR (400 MHz, $CDCl_3$), δ/ppm: 5.40 (s, 4H, CH_2), 6.93–6.98 (m, 4H, ArH), 7.00–7.05 (t, 4H, ArH), 8.11–8.15 (t, 1H, J = 8.0 Hz, pyridine proton), 8.48 (d, 2H, J = 8.0 Hz, pyridine protons); IR (KBr) v/cm: 3118, 1593, 1574, 1542, 1464, 1402, 1251, 1098, 1081, 687; MS (ESI) m/z (%): 599 (M + 23, 25), 598 (M + 22, 100), 576 (M, 30); Anal. Calcd. for $C_{25}H_{15}F_2N_9O_2S_2$: C, 52.17; H, 2.63; N, 21.90; S, 11.14. Found: C, 52.14; H, 2.53; N, 21.92; S, 11.11.

2,6-bis(6-((4-chlorophenoxy)methyl)-[1,2,4]triazolo[3,4-b][1,3,4]thiadiazol-3-yl)pyridine (L^6). White solid, yield 67%. m.p. 258 °C; ^{1}H NMR (400 MHz, $CDCl_3$), δ/ppm: 5.41 (s, 4H, CH_2), 6.93 (d, 4H, J = 8.8 Hz, ArH), 7.29 (d, 4H, J = 9.2 Hz, ArH), 8.11–8.15 (t, H, J = 7.8 Hz, pyridine proton), 8.48 (d, 2H, J = 8.0 Hz, pyridine protons); IR (KBr) v/cm: 3138, 1595, 1572, 1546, 1464, 1400, 1243, 1040, 709, 687; MS (ESI) m/z (%): 632 (M + 24, 83), 630 (M + 22, 100), 608 (M, 16); Anal. Calcd. for $C_{25}H_{15}Cl_2N_9O_2S_2$: C, 49.35; H, 2.48; N, 20.72; S, 10.54. Found: C, 49.60; H, 2.49; N, 20.47; S, 10.60.

2,6-bis(6-((4-bromophenoxy)methyl)-[1,2,4]triazolo[3,4-b][1,3,4]thiadiazol-3-yl)pyridine (L^7). Gray solid, yield 83%. m.p. 245 °C; ^{1}H NMR (400 MHz, $CDCl_3$), δ/ppm: 5.40 (s, 4H, CH_2), 6.88 (d, 4H, J = 9.2 Hz, ArH), 7.43 (d, 4H, J = 9.2 Hz, ArH), 8.11–8.15 (t, 1H, J = 7.8 Hz, pyridine proton), 8.48 (d, 2H, J = 8.0, pyridine protons); IR (KBr) v/cm: 3140, 1594, 1581, 1546, 1464, 1403, 1246, 1052, 680, 599; MS (ESI) m/z (%): 720 (M + 23,100), 718 (M + 21, 49), 698 (M + 1, 38), 696 (M – 1, 15); Anal. Calcd. for $C_{25}H_{15}Br_2N_9O_2S_2$: C, 43.06; H, 2.17; N, 18.08; S, 9.20. Found: C, 43.05; H, 2.14; N, 18.27; S, 9.34.

2,6-bis(6-((4-iodophenoxy)methyl)-[1,2,4]triazolo[3,4-b][1,3,4]thiadiazol-3-yl)pyridine (L^8). Black solid, yield 88%. m.p. 155 °C; ^{1}H NMR (400 MHz, $CDCl_3$), δ/ppm: 5.40 (s, 4H, CH_2), 6.76 (d, 4H, J = 9.2, ArH), 7.62 (d, 4H, J = 9.2 Hz, ArH), 8.11–8.15 (t, 1H, J = 8.0 Hz, pyridine proton), 8.48 (d, 2H, J = 8.4 Hz, pyridine protons); IR (KBr) v/cm: 3152, 1634, 1578, 1547, 1467, 1400, 1244, 1050, 680, 419; MS (ESI) m/z (%): 814 (M + 23, 100), 792 (M + 1, 14); Anal. Calcd. for $C_{25}H_{15}I_2N_9O_2S_2$: C, 37.94; H, 1.91; N, 15.93; S, 8.10. Found: C, 37.82; H, 1.93; N, 16.04; S, 8.18.

Synthesis of the target terbium complexes

The synthesis methods of target Tb^{3+} complexes were similar, so the synthesis of the Tb^{3+} complexes of compound L^1 is described as an example. The compound L^1 was dissolved in 30 mL chloroform at 80 °C, and 1.25 mL $Tb(NO_3)_3$ (0.2 mol/L) solution was added, then a large number of white precipitate was formed immediately. The reaction mixture was maintained at reflux for 4 h, the resulting solid complexes were collected by the hot filtration, and washed several times with chloroform. Finally, the target Tb^{3+} complex was dried under vacuum for 6 h.

Results and discussion

Elemental analysis and solubility of the target complexes

The compositions of eight Tb^{3+} complexes were confirmed on the basis of the elemental analysis and molar conductivity, and their data are summarized in Table 1, which are in accordance with the theoretical values calculated, indicating that the composition of the target complexes are $(TbL^{1-8}(NO_3))(NO_3)_2{\cdot}H_2O$. The molar conductivity values of the target complexes in dimethylformamide (DMF) solution are in the range of 155–204 $S{\cdot}cm^2/mol$, which indicated that the target complexes are 2 : 1 electrolytes (13). The results revealed that the possible chemical structure of the target complexes was shown in Fig. 1. The ligands $\mathbf{L^{1-8}}$ are very soluble in DMF and DMSO, and only partially soluble in chloroform, but insoluble in water, ethanol, benzene, etc., while the target complexes are only soluble in DMF and DMSO.

Ultraviolet spectra analysis

The UV absorption spectra of the ligands $\mathbf{L^{1-8}}$ and their corresponding Tb^{3+} complexes were recorded in DMSO solution, and the data are summarized in Table 2. As the UV absorption spectra of all target complexes are similar, so the UV spectra of ligand $\mathbf{L^8}$ as well as its corresponding Tb^{3+} complex is selected for illustration and shown in Fig. 2.

It can be seen from Table 2 and Fig. 2 that the transition absorption peaks of the target complexes compared to the corresponding ligands are all red-shifted; in particular, the $n \rightarrow \pi^*$ transitions absorption peak are all shifted to 308 nm, which are attributed to the impact of the central Tb^{3+} ion.

Figure 2 shows that there are two absorption peaks at 275 nm and 305 nm, which are ascribed to the π–π^* and n–π^* transitions in ligand $\mathbf{L^8}$, respectively. The UV spectrum of the complex $[TbL^8(NO_3)](NO_3)_2{\cdot}H_2O$ is very similar to that of the free ligand $\mathbf{L^8}$. The only difference is that the absorption intensity of the complex is decreased, which is attributed to Tb^{3+} ion that enlarged the ligand's conjugated system. This evidence shows that ligand $\mathbf{L^8}$ is coordinated successfully with the center Tb^{3+} ion (14).

Infrared spectra analysis

The IR data of all ligands and their corresponding Tb^{3+} complexes are presented in Table 3. The results show that the

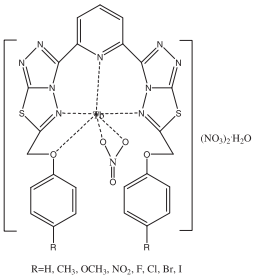

Figure 1. The possible chemical structure of the target complexes.

Table 2. Ultraviolet spectra data of complexes

Complexes	λ_{max} (nm)	Ligand	λ_{max} (nm)
$[TbL^1(NO_3)](NO_3)_2{\cdot}H_2O$	276,308	L^1	276,306
$[TbL^2(NO_3)](NO_3)_2{\cdot}H_2O$	278,308	L^2	277,307
$[TbL^3(NO_3)](NO_3)_2{\cdot}H_2O$	289	L^3	286
$[TbL^4(NO_3)](NO_3)_2{\cdot}H_2O$	267,308	L^4	267,307
$[TbL^5(NO_3)](NO_3)_2{\cdot}H_2O$	278,308	L^5	277,306
$[TbL^6(NO_3)](NO_3)_2{\cdot}H_2O$	279,308	L^6	277,306
$[TbL^7(NO_3)](NO_3)_2{\cdot}H_2O$	278,308	L^7	277,305
$[TbL^8(NO_3)](NO_3)_2{\cdot}H_2O$	277,308	L^8	275,305

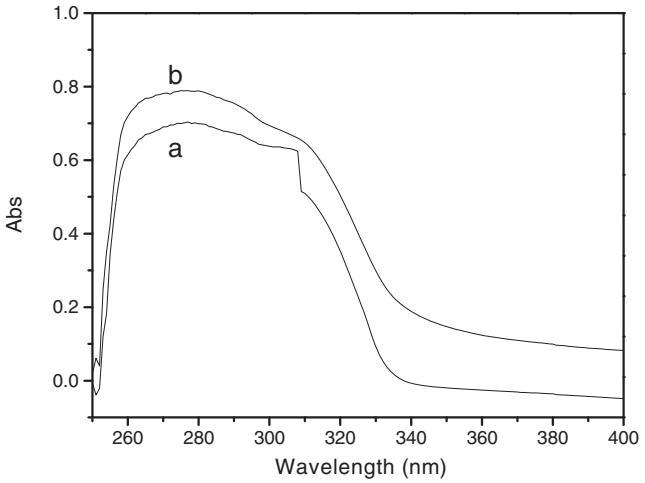

Figure 2. Ultraviolet spectra of the $[TbL^8(NO_3)](NO_3)_2{\cdot}H_2O$ (a) and the ligand L^8 (b).

Table 1. Elemental analysis and molar conductance data for target complexes

Complexes	Found (calculated) (%) C	H	N	Tb	Λ_m ($S{\cdot}cm^2/mol$)
$[TbL^1(NO_3)](NO_3)_2{\cdot}H_2O$	33.24 (33.22)	2.11 (2.10)	18.54 (18.60)	17.48 (17.61)	161
$[TbL^2(NO_3)](NO_3)_2{\cdot}H_2O$	34.78 (34.80)	2.49 (2.47)	18.01 (18.05)	17.26 (17.08)	174
$[TbL^3(NO_3)](NO_3)_2{\cdot}H_2O$	33.67 (33.64)	2.30 (2.39)	17.32 (17.45)	16.55 (16.51)	158
$[TbL^4(NO_3)](NO_3)_2{\cdot}H_2O$	30.17 (30.21)	1.71 (1.71)	19.58 (19.74)	16.21 (16.01)	192
$[TbL^5(NO_3)](NO_3)_2{\cdot}H_2O$	30.87 (31.95)	1.85 (1.81)	17.78 (17.89)	16.72 (16.93)	185
$[TbL^6(NO_3)](NO_3)_2{\cdot}H_2O$	30.78 (30.90)	1.72 (1.75)	17.23 (17.30)	16.18 (16.37)	155
$[TbL^7(NO_3)](NO_3)_2{\cdot}H_2O$	28.35 (28.30)	1.54 (1.60)	15.85 (15.85)	15.04 (15.00)	197
$[TbL^8(NO_3)](NO_3)_2{\cdot}H_2O$	26.25 (26.00)	1.38 (1.47)	14.58 (14.56)	13.72 (13.78)	204

LUMINESCENCE
The Journal of Biological and Chemical Luminescence

Table 3. Infrared spectra data of ligands and their corresponding terbium complexes

Compound	$\nu_{C=N}$	$\nu_{C=N-N}$	ν_{Ar-O-C}	ν_{C-S-C}	ν_{Ar-H}	ν_{OH}	νNO_3^{-1} ν_1	ν_4	ν_2	ν_3
L^1	1598	1246	1080	690	3138	3414				
$[TbL^1(NO_3)](NO_3)_2{\cdot}H_2O$	1598	1248	1081	690	3163	3397	1479	1388	1025	815
L^2	1590	1241	1083	685	3122	3413				
$[TbL^2(NO_3)](NO_3)_2{\cdot}H_2O$	1614	1238	1090	686	3130	3414	1484	1385	1028	815
L^3	1594	1232	1032	688	3121	3444				
$[TbL^3(NO_3)](NO_3)_2{\cdot}H_2O$	1615	1230	1030	688	3156	3411	1484	1385	1030	816
L^4	1611	1259	1053	687	3119	3413				
$[TbL^4(NO_3)](NO_3)_2{\cdot}H_2O$	1612	1261	1055	687	3138	3398	1487	1384	1022	816
L^5	1593	1251	1081	687	3118	3422				
$[TbL^5(NO_3)](NO_3)_2{\cdot}H_2O$	1615	1261	1097	688	3153	3400	1489	1388	1026	816
L^6	1595	1243	1040	687	3138	3414				
$[TbL^6(NO_3)](NO_3)_2{\cdot}H_2O$	1614	1246	1044	687	3140	3424	1480	1385	1027	818
L^7	1594	1246	1052	680	3140	3409				
$[TbL^7(NO_3)](NO_3)_2{\cdot}H_2O$	1615	1242	1070	680	3129	3409	1484	1385	1021	817
L^8	1634	1244	1050	680	3152	3429				
$[TbL^8(NO_3)](NO_3)_2{\cdot}H_2O$	1616	1241	1057	680	3194	3401	1480	1385	1029	817

IR spectra of ligands and corresponding complexes present similar features to each other, so the IR spectra of the free ligands **L^4** and **L^6** as well as their corresponding complexes $[TbL^4(NO_3)](NO_3)_2{\cdot}H_2O$ and $[TbL^6(NO_3)](NO_3)_2{\cdot}H_2O$ are selected for illustration and shown in Figs 3 and 4, respectively.

Figures 3 and 4 show that the free ligands **L^4** and **L^6** exhibit absorption bands at 1611/cm and 1595/cm respectively, which are assigned to the ν(C = N) stretching vibration of the pyridine ring, while, in their corresponding Tb^{3+} complexes, the absorption band shifts by about 2/cm and 19/cm to a higher frequency as compared to that of their counterpart for the free ligands **L^4** and **L^6**, respectively, which indicate that the nitrogen atom of the C = N group coordinates with the rare earth ion. The IR absorption spectra of ligands **L^4** and **L^6** are at 1053/cm and 1040/cm, which are attributed to the stretching vibration of the Ar-O-C group, but in their corresponding Tb^{3+} complexes, the Ar-O-C group stretching frequency are red-shifted to 1055/cm and 1044/cm, respectively. All these results indicate that the oxygen atom of Ar-O-C group coordinates with the rare earth ion (15). In the free ligands **L^4** and **L^6**, the C = N-N group stretching modes is appeared at 1259/ cm^{-1} and 1243/ cm^{-1}, but the shifting of the C = N-N stretching peak in the corresponding Tb^{3+} complexes to a longer wavelength indicates involvement of the nitrogen atom of the C = N-N group in coordination (16). While, the C-S-C group stretching vibration locates at around 685/cm in all ligands, but it is not obviously shifted in the target complexes. This evidence shows that the sulfur atom of the C-S-C group does not participate in coordination, which is ascribed to sterically hindered occurring, and the central ion is difficult to coordinate with the sulfur atom of the fused heterocyclic and nitrogen atom of the pyridine ring simultaneously. The above results reveal that the position of the characteristic IR absorption bands provides significant indications regarding bonding sites of the ligands when coordinating with the Tb^{3+} ion (17).

It is seen from Table 3 that the characteristic frequencies of the coordinating nitrate groups appeared approximately at 1481 (υ_1), 1324 (υ_4), 1031 (υ_2) and 815 cm (υ_3). In addition, the difference between the two strongest absorption bands of the

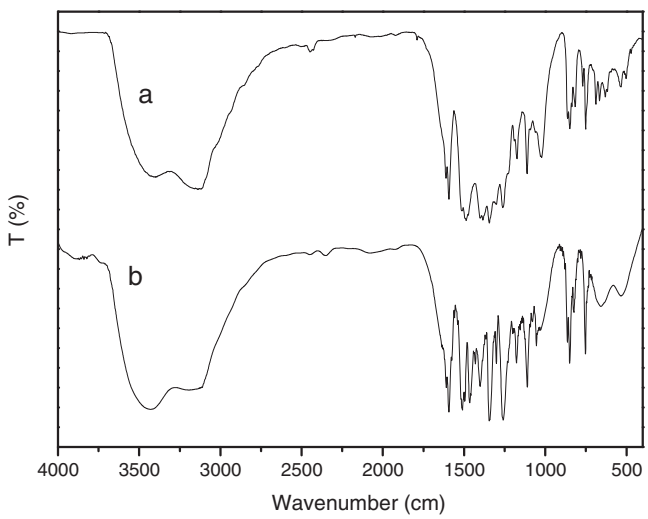

Figure 3. Infrared spectra of $[TbL^4(NO_3)](NO_3)_2{\cdot}H_2O$ (a) and L^4 (b).

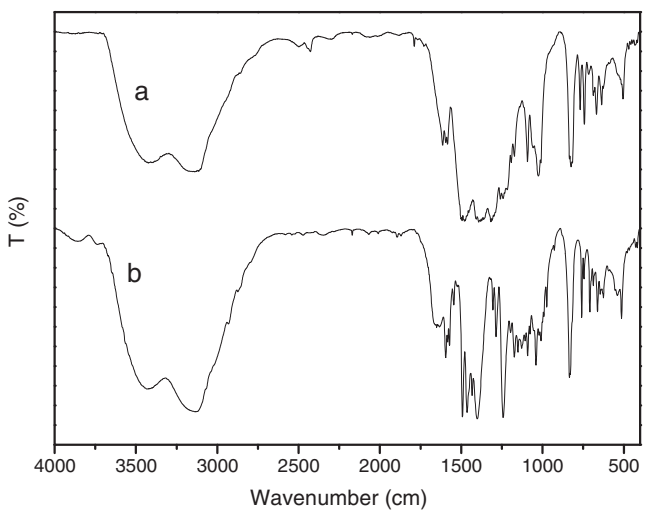

Figure 4. Infrared spectra of $[TbL^6(NO_3)](NO_3)_2{\cdot}H_2O$ (a) and L^6 (b).

nitrate groups ($|\upsilon_1-\upsilon_4|$) can be defined as $\Delta\nu$. It is generally believed that the $\Delta\nu$ value is below 200 for the bidentate nitrate moiety, but above 200 for the monodentate nitrate moiety (18). While, the $\Delta\nu$ values of $[TbL^4(NO_3)](NO_3)_2{\cdot}H_2O$ and $[TbL^6(NO_3)](NO_3)_2{\cdot}H_2O$ are about 103/cm and 95/cm, respectively, which indicate that the nitrate groups coordinate to the Tb^{3+} ion as bidentate ligands in the target complexes. Meanwhile, there are free nitrate groups in the target complexes, which are consistent with the results of the conductivity experiment, and confirmed in thermal gravimetric analyses. The broad absorption band of the –OH stretching vibration in the range 3398–3444/cm can be seen in free ligands and target complexes, which indicate that the presence of the water molecules adsorbed on to ligands, the complexes contained crystallization water, these results will be further confirmed in thermal gravimetric analyses.

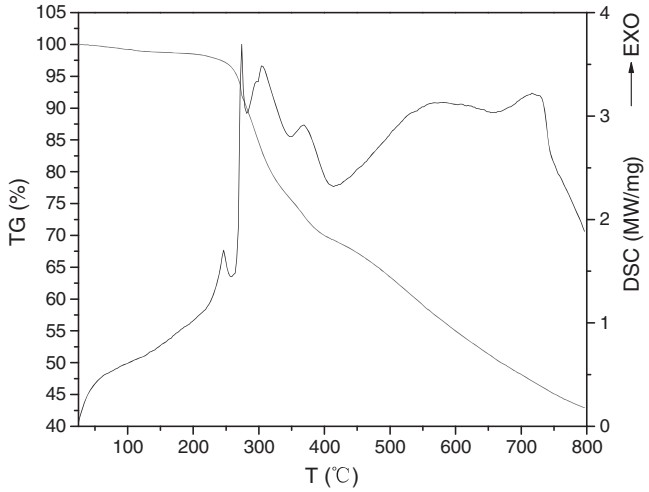

Figure 5. TG–DSC curves of $[TbL^5(NO_3)](NO_3)_2{\cdot}H_2O$. DSC, ?????; TG, thermogravimetric.

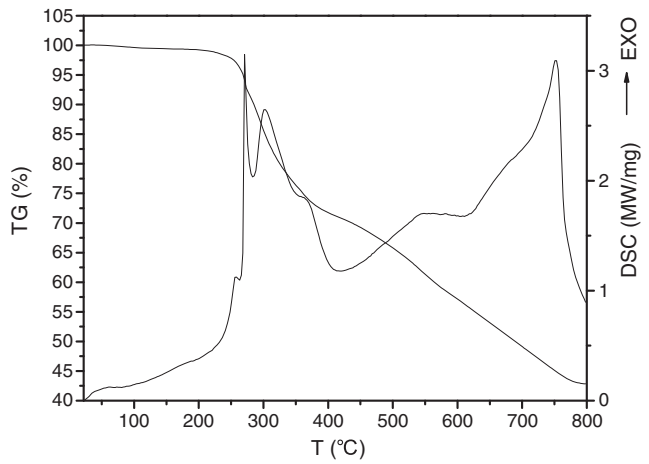

Figure 6. TG–DSC curves of $[TbL^6(NO_3)](NO_3)_2{\cdot}H_2O$. DSC, ?????; TG, thermogravimetric.

Thermal analysis

To investigate thermal stability and details of thermal decomposition of the target complexes, thermal analysis was carried out. The eight target complexes present similar thermal behavior, thus, in this paper, we only give the thermogravimetric and differential thermal analysis curves of $[TbL^5(NO_3)](NO_3)_2{\cdot}H_2O$ and $[TbL^6(NO_3)](NO_3)_2{\cdot}H_2O$ as examples for illustration, which are shown in Figs 5 and 6, respectively. The thermogravimetric analysis data were obtained at a heating rate of 10 °C/min and summarized in Table 4.

The thermogravimetric and differential thermal analysis analyses for complexes $[TbL^5(NO_3)](NO_3)_2{\cdot}H_2O$ and $[TbL^6(NO_3)](NO_3)_2{\cdot}H_2O$ were studied in the range of 20–800 °C. Figures 5 and 6 show that the weight losses during the first step for these complexes are 1.73% and 1.66% and between 70 and 150 °C. These values have good agreement with the loss of one lattice of water molecules depending on the complexes (19), and the calculated values are 1.92% and 1.85%, respectively. In addition, the target complexes are without endothermic peak and weightlessness at 150–230 °C, which illustrate that the water does not participate in coordination with the target complexes, because the coordination water of the analogous complexes is usually released over 200 °C. Although there are endothermic peaks of all complexes appearing in the vicinity 265 °C, but no apparent weightlessness, which is ascribed to the melt of target complexes. Meanwhile, there are weight loss steps at temperatures 284 °C and 348 °C with 13.30% and 6.65% for $[TbL^5(NO_3)](NO_3)_2{\cdot}H_2O$, 12.73% and 6.35% for $[TbL^6(NO_3)](NO_3)_2{\cdot}H_2O$, corresponding to the process that loss of the outside two molecules nitrate and internally a molecule nitrate of the target complexes, respectively, those values correspond with

Table 4. Thermal analysis data for target complexes

Complexes	Endothermic peak (°C)	H_2O (lost) (%)	NO_3^-(lost) (%)	Ligand (lost) (%)	Metal residue (%)
	Temp.	TG (Calcd.)	TG (Calcd.)	TG (Calcd.)	TG (Calcd.)
$[TbL^1(NO_3)](NO_3)_2{\cdot}H_2O$	90, 265, 460	2.15 (1.99)	20.16 (20.60)	35.18 (36.88)	42.58 (40.53)
$[TbL^2(NO_3)](NO_3)_2{\cdot}H_2O$	265, 372	1.62 (1.93)	19.83 (19.98)	36.14 (38.78)	43.02 (39.31)
$[TbL^3(NO_3)](NO_3)_2{\cdot}H_2O$	264, 337, 395	2.20 (1.87)	19.08 (19.31)	39.59 (40.81)	40.51 (38.01)
$[TbL^4(NO_3)](NO_3)_2{\cdot}H_2O$	241, 291, 408	1.97 (1.81)	18.82 (18.73)	38.32 (42.60)	42.16 (36.86)
$[TbL^5(NO_3)](NO_3)_2{\cdot}H_2O$	257, 284, 414	1.73 (1.92)	19.95 (19.81)	36.87 (39.29)	42.56 (38.98)
$[TbL^6(NO_3)](NO_3)_2{\cdot}H_2O$	263, 284, 415	1.66 (1.85)	19.08 (19.16)	38.16 (41.30)	42.04 (37.69)
$[TbL^7(NO_3)](NO_3)_2{\cdot}H_2O$	86, 266, 404	1.59 (1.70)	17.26 (17.55)	43.66 (46.22)	38.52 (34.53)
$[TbL^8(NO_3)](NO_3)_2{\cdot}H_2O$	96, 266, 435	1.96 (1.56)	16.15 (16.12)	50.72 (50.60)	31.60 (31.72)

TG, thermogravimetric analysis.

LUMINESCENCE
The Journal of Biological and Chemical Luminescence

the calculated values. The last weight loss step is at 414 °C for $[TbL^5(NO_3)](NO_3)_2{\cdot}H_2O$ and 415 °C for $[TbL^6(NO_3)](NO_3)_2{\cdot}H_2O$, and the weightlessness is 36.87% and 38.16%; these values are consistent with the calculated values of organic ligands decomposition, respectively. The target complexes are decomposed completely at 800 °C, and the remaining solid composition is Tb_2O_3 and its quality percentage is 42.56% for $[TbL^5(NO_3)](NO_3)_2{\cdot}H_2O$ and 42.04% for $[TbL^6(NO_3)](NO_3)_2{\cdot}H_2O$, which is identical to the calculated values 38.98% and 37.69%, respectively. The thermal analysis results show that the target complexes have high thermal stability, and are consistent with the results of other analyses.

Fluorescence properties analysis

The fluorescence properties of target complexes were determined on solid-state samples at room temperature, and both the excitation and emission light slits were 2.5 nm. The fluorescence spectra data of the target complexes are summarized in Table 5. The observed fluorescence spectra of all target complexes are very similar; the fluorescence spectrum of $[TbL^6(NO_3)](NO_3)_2{\cdot}H_2O$ was selected for illustration, and its excitation and emission spectra are shown in Figs 7 and 8, respectively.

It is seen from Fig. 7 that the excitation spectrum of $[TbL^6(NO_3)](NO_3)_2{\cdot}H_2O$, which was measured under an emission wavelength of 540 nm, possesses a broad excitation band with the strongest excitation peak at 364 nm. Meanwhile, Fig. 8 shows that the characteristic emission spectra of the target Tb^{3+} complex consisted of four main bands at approximately 491.5 nm ($^5D_4 \rightarrow {}^7F_6$), 545.5 nm ($^5D_4 \rightarrow {}^7F_5$), 585 nm ($^5D_4 \rightarrow {}^7F_4$) and 623 nm ($^5D_4 \rightarrow {}^7F_3$). It can be noted that there are narrow and sharp emission peaks appearing at approximately 491.5 nm, which indicates that the complexes have good monochromaticity and the ligand **L⁶** is a comparatively good organic chelator for the absorption and transfer of energy to the center Tb^{3+} ion (20).

Table 5 shows that the fluorescence intensity of complex $[TbL^4(NO_3)](NO_3)_2{\cdot}H_2O$ is the lower than that of other complexes, which is due to ligand **L⁴** having an electrophilic group (-NO_2). In addition, the fluorescence intensity of the complex $[TbL^{2,3}(NO_3)](NO_3)_2{\cdot}H_2O$ is better than that of the complex $[TbL^1(NO_3)](NO_3)_2{\cdot}H_2O$, which is attributed to ligands **L²** and **L³** having an activating group (-CH_3 and -OCH_3, respectively). The above results show that the electron-withdrawing groups on the ligands can decrease the fluorescence intensity of the corresponding target complexes, and this is due to

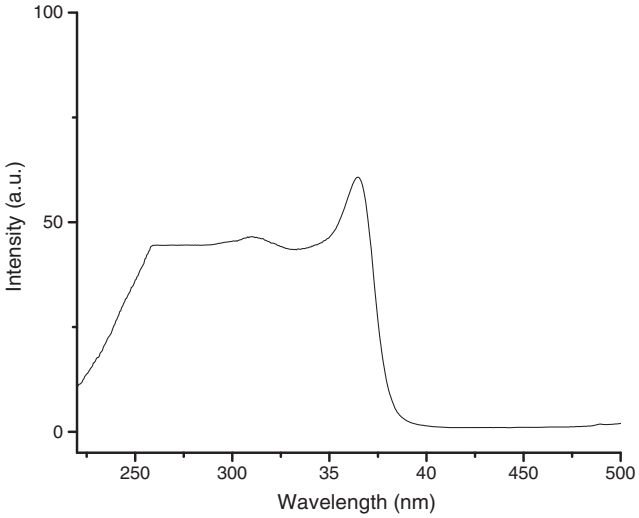

Figure 7. Excitation spectra of $[TbL^6(NO_3)](NO_3)_2{\cdot}H_2O$.

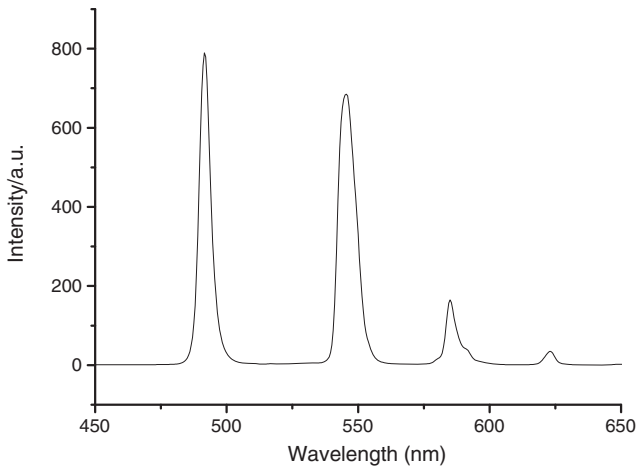

Figure 8. Emission spectra of $[TbL^6(NO_3)](NO_3)_2{\cdot}H_2O$.

(i) the electron-withdrawing groups can reduce electron density of the phenyl ring in the target complexes, and (ii), introduction of the electron-withdrawing groups can easily result in fluorescence quenching. On the contrary, the electron-donating groups on the ligands resulted in an increase in the fluorescence intensity of target complexes, which is due to the electron-donating groups donating electrons to the

Table 5. Fluorescence spectra data of the target terbium complexes

		$^5D_4 \rightarrow {}^7F_6$		$^5D_4 \rightarrow {}^7F_5$		$^5D_4 \rightarrow {}^7F_4$		$^5D_4 \rightarrow {}^7F_3$	
Complexes	λ_{ex} (nm)	λ_{em} (nm)	*I* (a.u.)	λ_{em} (nm)	*I* (a.u.)	λ_{em} (nm)	*I* (a.u.)	λ_{em} (nm)	*I* (a.u.)
$[TbL^1(NO_3)](NO_3)_2{\cdot}H_2O$	364	492	12.85	543.5	22.24	585	3.92	622.5	1.067
$[TbL^2(NO_3)](NO_3)_2{\cdot}H_2O$	364	491.5	492.8	545.5	441.6	585	103.9	623	22.02
$[TbL^3(NO_3)](NO_3)_2{\cdot}H_2O$	364	491.5	9.169	545.5	8.997	585	2.178	623	0.539
$[TbL^4(NO_3)](NO_3)_2{\cdot}H_2O$	364	491.5	1.219	545.5	1.547	585	0.434	623	0.117
$[TbL^5(NO_3)](NO_3)_2{\cdot}H_2O$	364	491.5	340.9	545.5	293.9	585	68.25	623	14.07
$[TbL^6(NO_3)](NO_3)_2{\cdot}H_2O$	364	491.5	789.3	545.5	685.3	585	165.1	623	34.73
$[TbL^7(NO_3)](NO_3)_2{\cdot}H_2O$	364	491.5	161.3	545.5	164.2	585	42.86	623	9.722
$[TbL^8(NO_3)](NO_3)_2{\cdot}H_2O$	364	491.5	28.69	545.5	26.69	585	6.684	623	1.565

aromatic ring and enlarging the π-conjugated system of the ligands. Whereas, the fluorescence intensity of complex $[TbL^{6}(NO_3)](NO_3)_2{\cdot}H_2O$ is the strongest in all target complexes, which is attributed to the following two factors. First, the chlorine atom has an inductive effect, resulting in the triplet level of ligand **L⁶** corresponding with the lowest excited state level of Tb^{3+} ions. Secondly, electrostatic factors in ligand–metal bonding, which may be affected by the counter anion in complexes, influenced the triplet state energy level (T_1) of the ligand **L⁶** and lowered this T_1 energy level in the target complexes. Thus, the triplet state energy level of **L⁶** in the Tb^{3+} complexes corresponds with the lowest excited state level of Tb^{3+}. In comparison with the complex $[TbL^{6}(NO_3)](NO_3)_2{\cdot}H_2O$, the fluorescence intensity of the complex $[TbL^{7\text{-}8}(NO_3)](NO_3)_2{\cdot}H_2O$ is relatively decreased, which is attributed to the heavy atom effect. Based on the theory of the antenna effect (21), the fluorescence intensity of the target complexes is related to the efficiency of the intramolecular energy transfer between the triple level of the ligands and the vibrational level of the rare earth ions, which depends on the energy gap (Eg) between the two levels. It is shown in Table 5 that the fluorescence intensity of complex $[TbL^{6}(NO_3)](NO_3)_2{\cdot}H_2O$ is the strongest in all target complexes, which demonstrate that the triplet level of the ligand **L⁶** correspond with the vibrational level of the rare earth ions in all target complexes. At the same time, all target complexes show characteristic lines for the sensitization of Tb^{3+} ions, which shows that the energy will be absorbed and transferred to central Tb^{3+} ions effectively. The above results further highlight that the nature of the substituted group has a significant effect upon the fluorescence intensity of the Tb^{3+} complexes.

Fluorescence quantum yields analysis

The fluorescence quantum yields (Φ_{fx}) of the target complexes were determined using a sulfuric acid solution (0.1 mol/L) of quinine sulfate (1.0 μg/mL) with a known quantum yield ($\phi_{fstd} = 0.55$) as standard reference at room temperature because of the similarly between its absorption and fluorescent spectra with those of the target complexes. The fluorescence quantum yields (Φ_{fx}) are calculated by a comparative method (22) using the following equation.

$$\Phi_{fx} = \frac{n_x^2}{n_{std}^2} \cdot \frac{F_x}{F_{std}} \cdot \frac{A_{std}}{A_x} \cdot \Phi_{fstd}$$

where n_x (1.48) and n_{std} (1.34) are the refractive indices of solvents used for the sample and standard. F_x and F_{std} are the areas under the fluorescence curves of the sample and the used standard. A_x and A_{std} are the absorbances of the sample and standard at the excitation wavelength, respectively, both the sample and standard are excited at the same relevant wavelength, so that the A_{std} is equal to the A_x. The fluorescence quantum yields data of all target complexes are summarized in Table 6.

As shown in Table 6, $[TbL^{2}(NO_3)](NO_3)_2{\cdot}H_2O$ exhibits the highest quantum yield (0.607), resulting from the larger donor character of the methyl moiety and larger π-conjugated system of the phenyl moiety. By contrast, $[TbL^{4}(NO_3)](NO_3)_2{\cdot}H_2O$ shows the lowest quantum yield (0.490), which is attributed to the n → π* transition of the electron-withdrawing group (-NO_2) substituent belongs to forbidden transition, the excited state molecules are seldom obtained. For the halogen-substituted target complexes, the fluorescence quantum yield of $[TbL^{6}(NO_3)](NO_3)_2{\cdot}H_2O$ is the highest among $[TbL^{5\text{-}8}(NO_3)](NO_3)_2{\cdot}H_2O$. Different from **L⁵** and **L⁷,⁸**, the ligand **L⁶** can induce an electronic rearrangement of the complexes, which may improve the energy level matching between the ligands and the central Tb^{3+} ions. The results reveal that the 4-position substituent on the benzene ring has a significant effect on the fluorescence quantum yields of the target complexes, the electron-donating substituents can increase the fluorescence quantum yields of the target complexes, on the contrary, electron-withdrawing groups can decrease the fluorescence quantum yields of the target complexes.

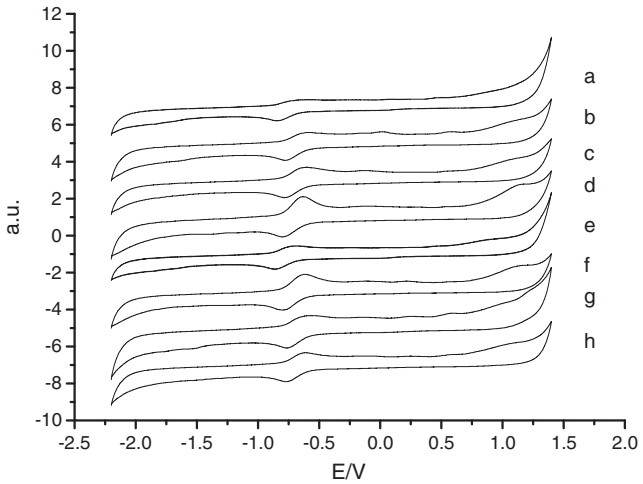

Figure 9. Oxidation potential of $[TbL^{1\sim8}(NO_3)](NO_3)_2{\cdot}H_2O$ (a–h).

Table 6. Fluorescence quantum yield data of the target complexes in dimethyl sulfoxide (1.0×10^{-6} mol/L)

Complexes	Excitation wavelength, λ (nm)	Fluorescence intensity, *I* (a.u.)	Fluorescence quantum yield (Φ)
$[TbL^{1}(NO_3)](NO_3)_2{\cdot}H_2O$	318	2048	0.585
$[TbL^{2}(NO_3)](NO_3)_2{\cdot}H_2O$	316	2606	0.607
$[TbL^{3}(NO_3)](NO_3)_2{\cdot}H_2O$	320	1731	0.562
$[TbL^{4}(NO_3)](NO_3)_2{\cdot}H_2O$	314	1327	0.490
$[TbL^{5}(NO_3)](NO_3)_2{\cdot}H_2O$	317	2095	0.594
$[TbL^{6}(NO_3)](NO_3)_2{\cdot}H_2O$	314	2193	0.598
$[TbL^{7}(NO_3)](NO_3)_2{\cdot}H_2O$	315	2062	0.588
$[TbL^{8}(NO_3)](NO_3)_2{\cdot}H_2O$	318	1886	0.571

LUMINESCENCE
The Journal of Biological and Chemical Luminescence

Table 7. Electrochemical data for terbium complexes

Complexes	λ_{onset} (nm)	Eox (v)	E_{HOMO} (ev)	Eg (ev)	E_{LUMO} (ev)
$[TbL^1(NO_3)](NO_3)_2{\cdot}H_2O$	254	0.677	5.417	4.882	0.535
$[TbL^2(NO_3)](NO_3)_2{\cdot}H_2O$	254	0.742	5.482	4.882	0.600
$[TbL^3(NO_3)](NO_3)_2{\cdot}H_2O$	251	0.705	5.445	4.940	0.505
$[TbL^4(NO_3)](NO_3)_2{\cdot}H_2O$	249	0.646	5.386	4.980	0.406
$[TbL^5(NO_3)](NO_3)_2{\cdot}H_2O$	251	0.658	5.398	4.940	0.458
$[TbL^6(NO_3)](NO_3)_2{\cdot}H_2O$	252	0.664	5.404	4.921	0.483
$[TbL^7(NO_3)](NO_3)_2{\cdot}H_2O$	250	0.670	5.410	4.960	0.450
$[TbL^8(NO_3)](NO_3)_2{\cdot}H_2O$	251	0.675	5.415	4.940	0.475

Electrochemical properties analysis

The electrochemical properties of the target complexes were investigated by means of a cyclic voltammetric technique in DMSO solution (23). The highest occupied molecular orbital (HOMO) and lowest unoccupied molecular orbital (LUMO) energy levels of the target complexes are estimated according to the electrochemical performance and the UV absorption spectra (24). The HOMO and LUMO data for target complexes are obtained using equation $E_{HOMO} = 4.74 + eE_{OX}$, $E_{LUMO} = Eg + E_{HOMO}$, $Eg = 1240/\lambda_{onset}(eV)$ (13) (λ_{onset} is the largest UV absorption spectra peak starting value). All cyclic voltammetrics are depicted in Fig. 9 and their electrochemical data are summarized in Table 7.

It is seen from Table 7 that the oxidation potential of all complexes occurs in the potential range +0.646 to +0.742 V. The Eg of all target complexes is between 4.882 eV and 4.980 eV. Compared with the complex $[TbL^1(NO_3)](NO_3)_2{\cdot}H_2O$, the oxidation potential and HOMO energy levels of complexes $[TbL^{2\text{-}3}(NO_3)](NO_3)_2{\cdot}H_2O$ are higher, and in contrast, that of the complexes $[TbL^{4-8}(NO_3)](NO_3)_2{\cdot}H_2O$ are lower; these phenomena are ascribed to the ligands $\mathbf{L^{2-3}}$ having electron-donating groups and $\mathbf{L^{4-8}}$ having electron-withdrawing groups. The oxidation potentials and HOMO energy levels of the Tb^{3+} complexes with halogen substituents are increased in the order of F < Cl < Br < I, the results show that introducing of electron-donating groups can increase the oxidation potential of the Tb^{3+} complexes, while introduction of an electron-withdrawing groups can reduce it. In other words, the nature of the substituent group can affect the HOMO energy levels of the target complexes. The frontier orbital theory (25) may provide an explanation for the above phenomena; the HOMO possesses the priority to provide electrons. For electron donor compounds, the oxidation process corresponds to the process of losing electrons in HOMO.

Conclusions

With 2,6-pyridine dicarboxylic acid as starting material, eight novel 1,2,4-triazolo[3,4-b]-1,3,4-thiadiazol derivatives have been synthesized by esterification, hydrazinolysis and cyclization successively, their corresponding Tb^{3+} complexes were prepared successfully, and characterized by means of elemental analysis, EDTA titrimetric, molar conductance, UV and Fourier transform-infrared spectrum as well as thermal performance studies. The fluorescent test results revealed that the target complexes emitted characteristic fluorescence of the Tb^{3+} ion, and the fluorescence intensity of the target complex with ligand substituted by chlorine is the strongest in all complexes. The electrochemical analysis results showed that the introduction of electron-donating groups can increase the oxidation potential and HOMO energy levels of the target complexes, and, introduction of electron-withdrawing groups can reduce the oxidation potential and HOMO energy levels of the target complexes. In addition, the thermal analysis provided information about the high thermal stability for the target complexes. In summary, the above results show that the target Tb^{3+} complexes are promising candidates for luminescent materials.

Acknowledgments

The authors are grateful for the financial support of the National Natural Science Foundation of China (no. J1103312), the Natural Science Foundation of Hunan Province (no. 11JJ5005) and the Innovative Research Team in University (no. IRT1238) as well as the Science and Technology Project of Hunan Provincial Science and Technology Department (no. 2012GK3156). We also thank Dr. William Hickey, the US Professor of HRM, for the English editing on this paper.

References

1. Wang DG, Yang YX, Yang YQ, Zhao TC, Wu X, Wang SK, et al. Synthesis and properties of a Pr(III) complex with 2-acetylbenzimidazoledehyde-glycine Schiff-base ligand. Chin Sci Bull 2006;51:785–90.
2. Gusev AN, Hasegawa M, Shimizu T, Fukawa T. Synthesis, structure and luminescence studies of Eu(III), Tb(III), Sm(III), Dy(III) cationic complexes with acetylacetone and bis(5-(pyridine-2-yl)-1,2,4-triazol-3-yl)propane. Inorg Chim Acta 2013;406:279–84.
3. Xiao SX, Zhang JJ, Li X, Li QG, Ren N, Li H. Thermochemical studies on complex of $[Sm(o\text{-}NBA)_3\ phen]_2$. J Rare Earths 2010;28:12–17.
4. Allendorf MD, Bauer CA, Bhakta RK, Houk RJT. Chem Soc Rev 2009;38:1330–5.
5. Zhang ZH, Okamura TA, Hasegawa Y, Kawaguchi H, Kong LY, Sun WY. Syntheses, Structures, and Luminescent and Magnetic Properties of Novel Three-Dimensional Lanthanide Complexes with 1,3,5-Benzenetriacetate. Inorg Chem 2005;44:6219–27.
6. Zhao M, Xi P, Gu X. Synthesis, characterization and fluorescence properties of a novel rare earth complex for anti-counterfeiting material. J Rare Earths 2010;28:75–8.
7. Marina AK, Vasilii AI, Alexey NK. 2-Mercaptobenzothiazolate complexes of rare earth metals and their electroluminescent properties. Org Electron 2009;10:623–30.
8. Sujith KV, Balakrishna K, Adithya A. Microwave mediated synthesis of non-carboxylic analogues of ibuprofen with improved pharmacological activity. Chin Chem Lett 2011;22:508–10.
9. Liu S-G, Su W-Y, Pan R-K. The synthesis and luminescence of europium (III) complex based on deprotonated 1-(4-ethyl-4H-thieno[3,2-b]indol-6-yl)-4,4,4-trifluorobutane-1,3-dionate and 1,10-phenanthroline. Spectrochim Acta A 2013;103:417–22.
10. Li W-X, Zheng Y-S, Chai W-J. Fluorescence emission mechanism and fluorescence p roperties of t ernary Tb(III) complex with d iphenyl sulphoxide and bipyridine. Luminescence 2011;26:754–61.

11. Shen L, Yang Z, Tang R. Synthesis, luminescence properties of Eu(III) and Tb(III) complexes with a novel aromatic carboxylic acid and their interactions with bovine serum albumin. Spectrochim Acta A 2012;98:170–7.
12. Palekar VS, Damle AJ, Shukla SR. Synthesis and antibacterial activity of some novel bis-1,2,4-triazolo[3,4-b]-1,3,4-thiadiazoles and bis-4-thiazolidinone derivatives from terephthalic dihydrazide. Eur J Med Chem 2009;44:5112–16.
13. Wang DQ, Wang XM, He QG, Zhou MY, Rui WW, Tao XT. Enhanced two-photon absorption of novel four-branched chromophore via vibronic coupling. Tetrahedron Lett 2008;49:5871–6.
14. Wang B-D, Yang ZY, Zhang D-W, Wang Y. Synthesis, structure, infrared and fluorescence spectra of new rare earth complexes with 6-hydroxy chromone-3-carbaldehyde benzoyl hydrazone. Spectrochim Acta A 2006;63:213–19.
15. Li WX, Zheng YS, Chai WJ. Fluorescence emission mechanism and fluorescence p roperties of t ernary Tb(III) complex with d iphenyl sulphoxide and bipyridine. Luminescence 2011;26:754–61.
16. Seena EB, Mathew N, Kuriakose M, Kurup MRP. Synthesis, spectral and EPR studies of oxovanadium(IV) complexes incorporating tridentate ONO donor hydrazone ligands: Structural study of one oxovanadium(V) complex. Polyhedron 2008;27:1455–62.
17. Anoop MR, Binil PS, Suma S, Sudarsanakumar MR. Synthesis and spectral characterization of lanthanide complexes with 1, 2-di-phenyl-4-butyl-3,5-pyrazolid inedione: Luminescent property of Tb(III) complex. J Rare Earths 2012;30:709–15.
18. Kai K, Haixia Z, Ruijun MA. Synthesis, characterization and enhanced luminescence of terbium complexes with 2-pyrazinecarboxylic acid and butanedioic acid by inert-fluorescent lanthanide ions. J Rare Earths 2013;31:32–6.
19. Caires FJ, Lima LS, Carvalho CT, Giagio RJ, Ionashiro M. Thermal behaviour of malonic acid, sodium malonate and its compounds with some bivalent transition metal ions. Thermochim Acta 2010;497:35–40.
20. Liu S-G, Pan R-K, Zhou X-P, Wen X-L, Chen Y-Z, Wang S, et al. Blue-light excitable europium(III) complex based on deprotonated 1-(9-ethyl-6,8-dimethyl-9H-carbazol-2-yl)-4,4,4-trifluorobutane-1,3-dionate and ,10-phenanthroline. Inorg Chim Acta 2013;395:119–23.
21. Vicentini G, Zinner LB, Zukerman-Schpector J, Zinner K. Luminescence and structure of europium compounds. Coordin Chem Rev 2000;196:353–82.
22. Fery-Forgues S, Lavabre D. J Chem Educ 1999;76:1260.
23. Ilhan S, Temel H, Yilmaz I. electrochemical studies of new macrocyclic Schiff base containing pyridine head and its metal complexes. J Organomet Chem 2007;692:3855–65.
24. Ge G, He J, Guo H, Wang F, Zou D. Highly efficient phosphorescent iridium (III) diazine complexes for OLEDs: Different photophysical property between iridium (III) pyrazine complex and iridium (III) pyrimidine complex. J Organomet Chem 2009;694:3050–7.
25. Fleming I. *Frontier Orbitals and Organic Chemical Reactions*. London: Wiley, 1976.